J|A|C|S
ARTICLES
Published on Web 03/07/2003

Equilibrium O_2 Distribution in the Zn^{2+}-Protoporphyrin IX Deoxymyoglobin Mimic: Application to Oxygen Migration Pathway Analysis

Lynn McNaughton, Griselda Hernández, and David M. LeMaster*

Contribution from the Wadsworth Center, New York State Department of Health and Department of Biomedical Sciences, University at Albany, SUNY, Empire State Plaza, Albany, New York 12201-0509

Received August 8, 2002; E-mail: lemaster@wadsworth.org

Abstract: Proton spin relaxation induced by the triplet ground state of O_2 in the zinc-containing diamagnetic analogue of sperm whale deoxymyoglobin has been measured as a function of oxygen concentration. As no covalent binding of oxygen to the metal occurs in the zinc species, the relaxation effects of O_2 on the protein ^{1}H resonances arise exclusively via much weaker noncovalent interactions. The relaxation effects at the amide proton sites are found to be highly localized and are derived almost exclusively from O_2 binding at the four previously identified xenon binding sites. Relative binding constants of 1.0, 0.08, 0.07, and 0.23 were determined for the Xe 1, Xe 2, Xe 3, and Xe 4 sites, respectively. In combination with earlier measurements of the kinetics of the heme binding of oxygen, these equilibria measurements enable a more detailed analysis of models characterizing O_2 entry and egress. A correlation is established between the fraction of O_2 which enters the Fe^{2+}-binding site via rotation of the distal histidine side chain (so-called "histidine gate") and the experimentally observable O_2 (or CO) lifetime in the Xe 1 site. A physiological role for these secondary oxygen binding sites is proposed in enhancing the efficiency of the O_2 association reaction by rendering more favorable its competition with water binding in the distal heme pocket.

Introduction

The X-ray structure of sperm whale myoglobin reveals no unhindered path for O_2 diffusion to the heme iron. Soon after the X-ray structures of both myoglobin and hemoglobin were reported, Perutz[1] and Chance[2] proposed the "histidine gate" model in which the side chain of the distal histidine swings away from the heme iron and out into solution generating an open solvent path for O_2 diffusion to the iron site. Support from this model has come from the observation of increasing rates of O_2 association at lower pH values with an apparent p*K* value similar to that of the distal histidine[3] and the effect of mutations at the histidine site on the O_2 association rate.[4−7] Crystal structures[8−10] with large iron coordinating groups in the distal site have demonstrated that the distal histidine side chain is displaced into the solvent phase.

On the other hand, low-temperature geminate recombination studies of myoglobin[11] have indicated more complexity in the kinetics of O_2 and CO association than would be anticipated from a simple histidine gate mechanism. In these experiments, the $Fe^{2+}-O_2$ (or $-$CO, $-$NO) bond is photolyzed, and the time course of $Fe^{2+}-O_2$ re-formation is then followed spectroscopically. The multiple kinetic phases observed in these experiments stimulated the proposal of a sequential binding pathway[12] in which O_2 initially enters into one or more internal binding sites before migrating to the distal pocket site where the covalent bond to iron is formed (Figure 1a). Although the observed kinetic behavior simplifies as the temperature is increased, at room-temperature O_2 geminate reassociation exhibits biexponential time dependence.[13] Both molecular dynamics simulations[14,15] and mutagenesis studies[16] have been proffered as support for a sequential mechanism. Others[13,17] have argued for extending the histidine gate model to a side path model (Figure 1b) which includes a dead-end C state. Elegant competitive

(1) Perutz, M. F.; Matthews, F. S. *J. Mol. Biol.* **1966**, *21*, 199−202.
(2) Chance, B.; Ravilly, A.; Rumen, N. *J. Mol. Biol.* **1966**, *17*, 525−534.
(3) Tian, W. D.; Sage, J. T.; Champion, P. M. *J. Mol. Biol.* **1993**, *233*, 155−166.
(4) Springer, B. A.; Egeberg, K. D.; Sligar, S. G.; Rohlfs, R. J.; Mathews, A. J.; Olson, J. S. *J. Biol. Chem.* **1989**, *264*, 3057−3060.
(5) Rohlfs, R. J.; Mathews, A. J.; Carver, T. E.; Olson, J. S.; Springer, B. A.; Egeberg, K. D.; Sligar, S. G. *J. Biol. Chem.* **1990**, *265*, 3168−3176.
(6) Eich, R. F.; Li, T.; Lemon, D. D.; Doherty, D. H.; Curry, S. R.; Aitken, J. F.; Mathews, A. J.; Johnson, K. A.; Smith, R. D.; G. N. Phillips, J.; Olson, J. S. *Biochemistry* **1996**, *35*, 6976−6983.
(7) Scott, E. E.; Gibson, Q. H.; Olson, J. S. *J. Biol. Chem.* **2001**, *276*, 5177−5188.
(8) Bolognesi, M.; Cannillo, E.; Ascenzi, P.; Giacometti, G. M.; Merli, A.; Brunori, M. *J. Mol. Biol.* **1982**, *158*, 305−315.
(9) Ringe, D.; Petsko, G. A.; Kerr, D.; Montellano, P. R. O. d. *Biochemistry* **1984**, *23*, 2−4.
(10) Johnson, K. A.; Olson, J. S.; Phillips, G. N. J. *J. Mol. Biol.* **1989**, *207*, 459−463.
(11) Austin, R. H.; Beeson, K.; Eisenstein, L.; Frauenfelder, H.; Gunsalus, I. C.; Marshall, V. P. *Science* **1973**, *181*, 541−543.
(12) Austin, R. H.; Beeson, K. W.; Eisenstein, L.; Frauenfelder, H. *Biochemistry* **1975**, *14*, 5355−5373.
(13) Chatfield, M. D.; Walda, K. N.; Magde, D. *J. Am. Chem. Soc.* **1990**, *112*, 4680−4687.
(14) Tilton, R. F.; Singh, U. C.; I. D. Kuntz, J.; Kollman, P. A. *J. Mol. Biol.* **1988**, *199*, 195−211.
(15) Elber, R.; Karplus, M. *J. Am. Chem. Soc.* **1990**, *112*, 9161−9175.
(16) Huang, X.; Boxer, S. G. *Nat. Struct. Biol.* **1994**, *1*, 226−229.
(17) Scott, E. E.; Gibson, Q. H. *Biochemistry* **1997**, *36*, 11909−11917.

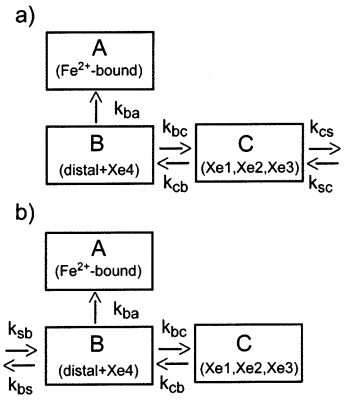

Figure 1. Sequential (a) and side path (b) models for myoglobin binding and release of O_2 to the solvent phase. These models differ as to whether oxygen leaves the distal pocket site directly into the solvent phase (k_{bs}) or via a secondary binding site (k_{cs}). For identification of the kinetic states with specific xenon binding sites, see text. Thermal dissociation of the Fe^{2+}–O_2 bond is negligible in the time frame of the photolytic geminate recombination experiments.

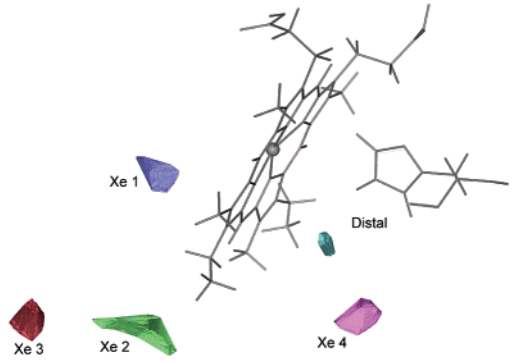

Figure 2. Cavities surrounding the heme and distal histidine side chain of deoxymyoglobin. A 0.1 Å grid search was carried out for the room-temperature 1.15 Å X-ray structure of sperm whale deoxymyoglobin[23] to determine the set of points at which the center of mass of an O_2 molecule could be positioned without steric overlap with the protein atoms. These cavities correspond closely to those previously identified as xenon binding sites[18] [Xe 1 (purple), Xe 2 (green), Xe 3 (red), Xe 4 (magenta) sites as well as the distal pocket (cyan)]. The water molecule in the distal pocket was removed in the calculation which otherwise occludes the distal pocket cavity.

xenon binding effects on recombination kinetics[17] as well as mutagenesis studies[7] have been cited in support of the side path model.

Parallel studies have attempted to identify the structural correlates of these proposed kinetic states. Petsko and co-workers[18] observed that, in addition to the previously observed[19] major xenon binding site on the proximal side of the heme (i.e. Xe 1), another binding site is contiguous with the distal pocket (Xe 4). The Xe 2 site lies at the edge of the heme ring along a potential pathway between the Xe 4 and Xe 1 sites, while the Xe 3 site branches away from Xe 2 (Figure 2). No xenon binding was observed near the iron in the distal pocket. Unambiguous identification of the individual kinetic states of O_2 and CO migration with specific xenon sites has been proven difficult. In part, this difficulty reflects the fact that for a given set of experimental conditions a single kinetic state may arise from O_2 bound in several distinct locations. In particular, the kinetic state B arises from all O_2 binding sites that exchange with each other on a time scale which is rapid compared to the rebinding to Fe^{2+} (k_{ba}), migration to the C state (k_{bc}), or movement out into solvent (k_{bs}).

Cryocrystallography on myoglobin crystals photolyzed at a series of increasing temperatures has indicated a sequence of CO migration steps from the distal pocket, to the Xe 4 site, and then at temperatures above 160−180 K to the Xe 1 site.[20,21] Subsequently, time-resolved Laue diffraction at room temperature[22] demonstrated that CO transfer to the Xe 1 region occurs in the time frame of 100 ns consistent with the kinetics of the B to C state transition.

Determination of relative contributions of the side path vs sequential mechanisms to the total O_2 migration has remained problematic. The two amplitudes and two time constants of the biexponential room-temperature O_2 geminate recombination kinetics can be fitted by the four parameters that characterize either the side path ($k_{ba} = 5.7$, $k_{bc} = 4.0$, $k_{cb} = 3.3$, $k_{bs} = 6.3$ μs^{-1}) or sequential ($k_{ba} = 5.7$, $k_{bc} = 10.3$, $k_{cb} = 1.3$, $k_{cs} = 2.0$ μs^{-1}) models.[7] As the amplitude of the slower phase is only 25% of that of the faster phase and the time separation is only a factor of ~8,[17] a significant range of parameters sets is consistent with the estimated experimental uncertainty of the recombination measurements. This uncertainty in the derived kinetic parameters is exacerbated by a substantial degree of correlation among the model variables. Although the experimental recombination kinetics can be equally well fitted by either model, the relative equilibrium O_2 binding for states B and C predicted by the optimal parameters differs markedly for the side path ($k_{bc}/k_{cb} = 1.2$) vs sequential model ($k_{bc}/k_{cb} = 7.9$). Direct determination of the relative equilibrium O_2 binding constants for the B and C states can serve to constrain these recombination kinetic parameters.

O_2 association from the bulk phase is not a simple reversal of the dissociation process monitored in the geminate recombination experiments. In place of the Fe^{2+}-bound O_2, deoxymyoglobin has a highly conserved water molecule hydrogen bonded to the distal histidine, which in the sperm whale X-ray structure has an occupancy of 0.6 at both room temperature[23] and 100 K.[24] Histidine side chain hydrogen bonding to Fe^{2+}-bound O_2 is believed to be critical for affinity and for the efficient discrimination against CO.[25] Water binding is generally viewed as an adventitious competition with O_2 binding. The additional kinetic constraint derived from equilibrium O_2 affinity measurements can enable a formally overdetermined analysis of the simple sequential and side path models and provide a more robust basis for incorporating the kinetic effects of competitive water binding.

Recently, we[26] reported that the paramagnetically induced relaxation of structurally buried amide ^1H resonances of the heat

(18) Tilton, R. F.; Kuntz, I. D.; Petsko, G. A. *Biochemistry* **1984**, *23*, 2849−2857.
(19) Schoenborn, B. P.; Watson, H. C.; Kendrew, J. C. *Nature* **1965**, *207*, 28−30.
(20) Chu, K.; Vojtchovsky, J.; McMahon, B. H.; Sweet, R. M.; Berendzen, J.; Schlichting, I. *Nature* **2000**, *403*, 921−923.
(21) Ostermann, A.; Waschipky, R.; Parak, F. G.; Nienhaus, G. U. *Nature* **2000**, *404*, 205−208.
(22) Srajer, V.; Ren, Z.; Teng, T.-Y.; Schmidt, M.; Ursby, T.; Bourgeois, D.; Pradervand, C.; Schildkamp, W.; Wulff, M.; Moffat, K. *Biochemistry* **2001**, *40*, 13802−13815.
(23) Kachalova, G. S.; Popov, A. N.; Bartunik, H. D. *Science* **1999**, *284*, 473−476.
(24) Vojtechovsky, J.; Chu, K.; Berendzen, J.; Sweet, R. M.; Schlichting, I. *Biophys. J.* **1999**, *77*, 2153−2174.
(25) Springer, B. A.; Sligar, S. G.; Olson, J. S.; Phillips, G. N. *J. Chem. Rev.* **1994**, *94*, 699−714.

stable rubredoxin protein can be quantitatively predicted from the time-averaged O_2 spatial distribution. Modulation of the electron−nuclear dipolar interaction is dominated by the 7.5 ps electron longitudinal relaxation rate,[27,28] which is rapid compared to either translational or rotational diffusion, thus rendering molecular motion comparatively ineffective in inducing relaxation. Furthermore, the electron T_1 value is insensitive to variations in the local noncovalent environment.[28] The ability to predict the magnitude of the relaxation effects arising from long-range interactions with oxygen molecules in the bulk solvent phase indicated the potential to use the paramagnetically induced relaxation for accurate determination of the distribution of O_2 bound within the protein interior.

Experimental Section

The molar relaxivity of O_2 at 14.1 T was determined directly on a 93% ^1H_2O, 7% ^2H_2O sample equilibrated under 100 psi excess pressure of O_2 at 21 °C vs an N_2-saturated sample. ^1H_2O T_1 values were determined for these samples by inversion recovery using a detuned probehead. A difference of 0.933 ± 0.005 s^{-1} for the 100 psi O_2 vs N_2 samples at 37 °C was obtained for measurements in triplicate. Given the O_2 solubility of 0.02337 v/v at 760 mmHg of gaseous O_2 at 37 °C,[29] correction for the pressure differential at 37 °C and the water vapor pressure yields an O_2 solution concentration of 7.43 ± 0.07 mM. The resultant O_2 relaxivity for the ^1H water resonance at 14.1 T is 126 ± 2 M^{-1}. Parallel measurements on these samples at 10 °C yielded a 69% increase in the O_2-induced relaxation of ^1H_2O, which is similar to the calculated 63% increase in the O_2 concentration. The corresponding estimate of 130 ± 3 M^{-1} for the molar relaxivity is consistent with the anticipated absence of a significant temperature dependence in the O_2 electron T_1.

Recombinant U-^2H,^{15}N-labeled sperm whale apo-myoglobin was expressed in *Escherichia coli* and purified through the hemin reconstitution step as previously described,[30] using 0.2% U-^2H glycerol as carbon source (expression plasmid kindly provided by J. Flanagan, Brookhaven National Laboratory). A 40−90% ammonium sulfate fractionation was followed by G-75 column gel filtration, heme extraction,[31] dialysis, reconstitution with Zn^{2+}-protoporphyrin IX, and purification on a CM-52 salt gradient column. All steps following the addition of the light-sensitive protoporphyrin were carried out under weak red light illumination. The 1 mM NMR sample in 50 mM KH_2PO_4, pH 7.1, was first equilibrated against 2 atm N_2 and then against 0.62, 1.73, and 7.65 mM O_2 as described.[26]

NMR samples were incubated for several days before data collection at 37 °C to allow for equilibration of the protoporphyrin orientation.[32] The backbone assignments were verified against those of CO−myoglobin[33] using a 3D $^{15}N-^{15}N-^1H$ HMQC-NOESY-TROSY experiment at 14.1 T. This experiment was based on a related pulse sequence[34] that was modified to eliminate the final ^1H 180° pulse in the TROSY refocusing period.[35,36] In addition, 3D $^1H-^{15}N-^1H$ HMQC-NOESY-HSQC and 3D $^1H-^{15}N-^1H$ HMQC-TOCSY-HSQC experiments[37] were carried out on a parallel ^{15}N-labeled Zn^{2+}-protoporphyrin IX myoglobin sample. ^1H T_1 values were obtained from $^1H-^{15}N$ TROSY experiments[38,39] with a purge pulse[40] at the beginning of the recycle delay to equalize ^1H recovery, solvent presaturation to suppress magnetization transfer from the solvent resonance, and phase cycling on the first ^1H 90° pulse to suppress ^{15}N magnetization contributions. Relaxation delay intervals of 0.1, 0.15, 0.25, 0.4, 0.6, 1.0, 1.5, 2.5, 4.0, 6.0, and 10.0 s were acquired for each sample. Exponential fits to the relaxation buildups yielded a median rmsd of 0.9% for the four data sets. The paramagnetically induced relaxation effects at the individual amide sites were estimated from the average differential between the O_2 and N_2 samples for at least two different O_2 concentrations. An average experimental uncertainty of 3.7% was obtained. Cavity calculations and grid summation of the dipolar relaxation effects were carried out as described previously[26] on the 1.15 Å resolution room-temperature X-ray structure of sperm whale deoxymyoglobin (1BZP).[23]

The biexponential fit to the 2 μs time course of the experimental O_2 geminate recombination data at 20 °C, pH 7.0,[7] served as reference for all simulation analyses. Numerical integration with a 0.2 ns step interval was used to determine sets of kinetic parameters which reproduced the reference data to within 1% rmsd. Reflecting the relative sensitivity of the simulations to the individual parameters, grid spacings of 0.05 μs^{-1} were used for k_{ba} and k_{cs}, 0.1 μs^{-1} for k_{bs}, and 0.15 μs^{-1} for k_{bc}. Bulk phase association kinetics were simulated up to 99% saturation at 0.2 mM O_2 using a 0.1 μs step interval for $k_{bc} < 6$ μs^{-1}, a 0.05 μs step for k_{bc} up to 12 μs^{-1}, and a 0.025 μs step for higher rates.

Results

O_2-Induced Paramagnetic Relaxation Measurements. Recombinant ^2H,^{15}N-labeled sperm whale myoglobin was prepared with Zn^{2+}-protoporphyrin IX substituted for the native heme. Although no crystal structure is available to date, the zinc substitution is generally regarded to provide a faithful structural mimic of the deoxy state.[41,42] Despite the higher pH (7.1) used in this study, the backbone resonance assignments of the Zn^{2+}-protoporphyrin IX myoglobin followed those published for CO-bound myoglobin.[33] The zinc-substituted myoglobin offers the combined benefits of a diamagnetic spin system and the absence of covalent O_2 binding to the metal site.[43] Thus, the observed paramagnetically induced relaxation effects arise only from the far weaker interactions of the noncovalently bound oxygen molecules.

Amide ^1H T_1 relaxation values were determined by variation of the relaxation delay period in a series of ^1H,^{15}N TROSY experiments.[38,39] Measurements were carried out on the myoglobin sample following equilibration against 0.62, 1.73, and 7.65 mM O_2 and the corresponding ^1H T_1 relaxation rates from an N_2-saturated data set were subtracted. In Figure 3 is illustrated a portion of the $^1H-^{15}N$ correlation spectra under N_2 atmosphere (panel a) and 1.73 mM O_2 (panel b). The latter condition corresponds to equilibration against ~2 atm O_2. With a median ^1H T_1 value of 3.3 s under N_2 atmosphere, the majority of amide resonances have recovered less than 5% of their equilibrium magnetization for the 0.15 s relaxation delay shown here. As is

(26) Hernandez, G.; Teng, C.-L.; Bryant, R. G.; LeMaster, D. M. *J. Am. Chem. Soc.* **2002**, *124*, 4463−4472.
(27) Hausser, R.; Noack, F. *Z. Naturforsch.* **1965**, *20a*, 1668−1675.
(28) Teng, C. L.; Hong, H.; Kiihne, S.; Bryant, R. G. *J. Magn. Reson.* **2001**, *148*, 31−34.
(29) Douglas, E. *J. Phys. Chem.* **1964**, *68*, 169−174.
(30) Shu, F.; Ramakrishnan, V.; Schoenborn, B. P. *Proc. Natl. Acad. Sci. U.S.A.* **2000**, *97*, 3872−3877.
(31) Teale, F. W. J. *Biochim. Biophys. Acta* **1959**, *35*, 543.
(32) LaMar, G. N.; Budd, D. L.; Viscio, D. B.; Smith, K. M.; Langry, K. C. *Proc. Natl. Acad. Sci. U.S.A.* **1978**, *75*, 5755−5759.
(33) Theriault, Y.; Pochapsky, T. C.; Dalvit, C.; Chiu, M. L.; Sligar, S. G.; Wright, P. E. *J. Biomol. NMR* **1994**, *4*, 491−504.
(34) Xia, Y. L.; Sze, K. H.; Zhu, G. *J. Biomol. NMR* **2000**, *18*, 261−268.
(35) Dingley, A. J.; Grzesiek, S. *J. Am. Chem. Soc.* **1998**, *120*, 8293−8297.
(36) Loria, J. P.; Rance, M.; Palmer, A. G. I. *J. Magn. Reson.* **1999**, *141*, 180−184.
(37) Talluri, S.; Wagner, G. *J. Magn. Reson., Ser. B* **1996**, *112*, 200−205.
(38) Pervushin, K.; Riek, R.; Wider, G.; Wuthrich, K. *Proc. Natl. Acad. Sci. U.S.A.* **1997**, *94*, 12366−12371.
(39) Weigelt, J. *J. Am. Chem. Soc.* **1998**, *120*, 10778−10779.
(40) Muhandiram, D. R.; Xu, G. Y.; Kay, L. E. *J. Biomol. NMR* **1993**, *3*, 463−470.
(41) Scheidt, R. W.; Reed, C. A. *Chem. Rev.* **1981**, *81*, 543−555.
(42) Hwang, Y.; Doyle, M. L.; Ackers, G. K. *Biophys. J.* **1996**, *71*, 2094−2105.
(43) Simolo, K.; Stucky, G.; Chen, S.; Bailey, M.; Scholes, C.; McLendon, G. *J. Am. Chem. Soc.* **1985**, *107*, 2865−2872.

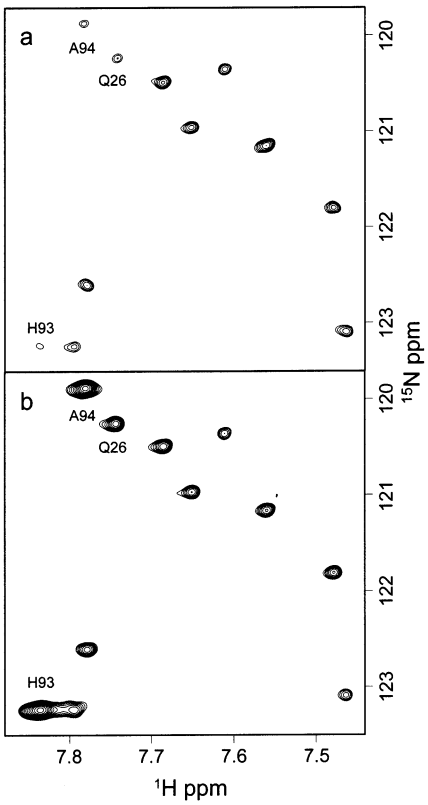

Figure 3. Relaxation effect of O_2 on selected amide ^1H resonances of Zn^{2+}-protoporphyrin IX myoglobin. Indicated is a portion of the $^1H-^{15}N$ correlation spectra under N_2 atmosphere (panel a) and 1.73 mM O_2 (panel b). For the 0.15 s relaxation recovery period used in these spectra the majority of resonances for the N_2-saturated sample have regained less than 5% of their equilibrium magnetization. Introduction of O_2 has little apparent effect on the majority of resonances. In contrast, the resonances of His 93, Ala 94, and to a lesser degree Gln 26 recover far more rapidly toward their equilibrium magnetization in the presence of O_2.

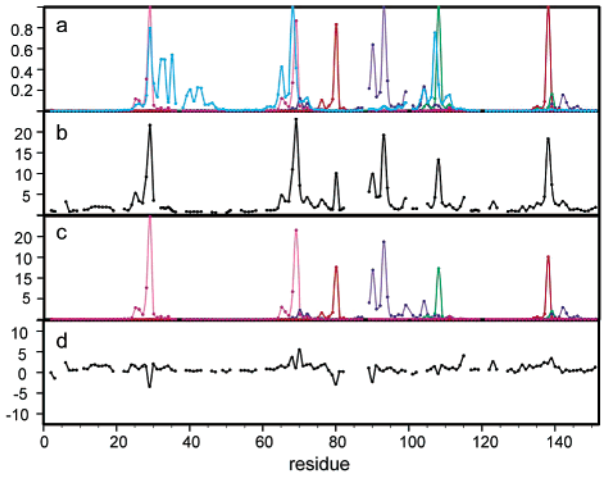

Figure 4. Observed and predicted O_2-induced relaxation of amide protons in Zn^{2+}-protoporphyrin IX myoglobin. Panel b indicates the difference in relaxation values of the O_2 vs N_2 saturated samples at 37 °C and pH 7.1 normalized to that of the solvent ^1H_2O resonance. Data are unavailable at amide sites undergoing rapid hydrogen exchange at these conditions. Dipolar relaxation effects of O_2 bound to the Xe 1 (purple), Xe 2 (green), Xe 3 (red), and Xe 4 (magenta) sites and to the distal pocket (cyan) at each amide proton were calculated by a $1/r^6$-weighted distance averaging for each cavity normalized to the maximum value (panel a) and scaled to the experimental relaxation data for the four xenon sites (panel c). Panel d indicates the difference between panels b and c.

most readily apparent for the amides of His 93 and Ala 94 near the Xe 1 cavity, the presence of 1.73 mM O_2 can greatly accelerate the rate of magnetization recovery.

A small set of structurally buried amides exhibit relaxation effects up to 25-fold greater than that for the ^1H_2O resonance (Figure 4b). On the other hand, the majority of amides show little O_2-induced relaxation beyond that predicted from oxygen in the bulk phase. This pattern of relaxation effects stands in marked contrast to that previously observed for the rubredoxin proteins.[26] In that case, no structurally buried amide proton exhibited an O_2-induced relaxation rate more than 60% that of the ^1H_2O solvent resonance, a 40-fold smaller relaxation effect than is observed for a subset of the myoglobin amides. The much weaker relaxation effects observed for rubredoxin were shown to arise almost exclusively from O_2 molecules in the bulk phase, consistent with the absence of any internal cavities large enough to accommodate an O_2 molecule which are not occupied by a highly ordered water molecule in the high-resolution X-ray structure. The striking elevation and nonuniformity of the relaxation effects observed for myoglobin indicate that a significant fraction of O_2 enters the protein interior and the internal distribution is highly localized.

Cavity O_2 Binding Constant Determination. Due to the short O_2 electron T_1, the simple $\langle 1/r^6 \rangle$ dependence of the paramagnetically induced relaxation effect facilitates modeling the relaxation arising from binding to the known internal cavities of myoglobin. The deoxymyoglobin structure has preexisting cavities which are only modestly perturbed by the binding of xenon atoms.[18] Cavity calculations on the 1.15 Å room-temperature deoxymyoglobin X-ray structure[23] were used to estimate the O_2-induced relaxation effect arising from oxygen bound to each of the xenon sites as well as to the distal pocket. The unit normalized values of the $1/r^6$-weighted averages for each cavity are given in Figure 4a. Each of the xenon binding sites predicts large O_2-induced relaxation effects only at the same amide positions for which such relaxation effects are observed. In contrast, the relaxation behavior predicted for the distal pocket cavity (cyan) does not correlate with the observed relaxation pattern of Figure 4b as is most apparent for the region of residues 32−45. This result is suggestive of a relatively low O_2 occupancy, consistent with the absence of observed xenon binding at this site.[18]

The relative O_2 binding constant estimates for each of the four xenon sites can be obtained directly from the scaling of the model relaxation data of panel a against the experimental data of panel b. It should be noted that only the relative binding constants enter into the analysis of the geminate recombination data considered below.

There are 8 amide sites near Xe 1 and 6 amide sites near Xe 4 which have predicted $\langle 1/r^6 \rangle$ values that are at least 10% of the maximum value (i.e. 0.1 in Figure 4a) and which have less than 10% of the site's predicted intensity arising from the other three xenon sites. Optimizing the predicted fits to these 14 amide sites yields scale factors of 18.7 and 24.5 for Xe 1 and Xe 4, respectively. Analogous calculations yield values of 12.1 and 15.3 for Xe 2 and Xe 3 (panel 4c). Subtraction of panel c from panel b indicates that the great majority of the observed relaxation behavior is adequately rationalized by this analysis (panel 4d). Monte Carlo simulations were carried out to estimate the uncertainty in these scale factors utilizing the 3.7% average experimental uncertainty for the individual amide ^1H relaxation

values of panel 4b. Uncertainty values of 0.5 and 0.6 were obtained for Xe 1 and Xe 4, respectively, while the less precisely determined Xe 2 and Xe 3 values had uncertainty values at least 2-fold larger.

Although each of the four xenon sites yield comparable relaxation effects, their relative O_2 occupancy varies substantially more, reflecting the differences in the distance to the nearest amide proton which range from 3.7 Å for Xe 3 to 5.6 Å for Xe 1. Relative to the Xe 1 site, the occupancies of Xe 2, Xe 3, and Xe 4 are estimated to be 0.081 ± 0.006, 0.066 ± 0.007, and 0.225 ± 0.009. These uncertainty estimates reflect only the accuracy of the experimental relaxation measurements and not the reliability of the O_2 distribution modeled from the static cavities of the 1.15 Å room-temperature X-ray structure.[23] To provide a measure of the sensitivity of these occupancy estimates to the details of the cavity model, a parallel analysis was carried out using the coordinates for the 100 K high-resolution X-ray structure.[24] Relative occupancies in the Xe 2, Xe 3, and Xe 4 sites of 0.210, 0.090, and 0.256 were obtained.

The resultant fit to the experimental relaxation data of panel 4b is significantly poorer using the low-temperature coordinate set. The absolute value of the residuals in the difference plot of panel 4d for the 8 amides optimized for Xe 1 is 13% of the initial intensity. This value increases to 24% when the 100 K X-ray coordinates are used. Similarly, the residuals for the fit to Xe 4 increase from 17% to 26% in going from the room temperature to the low temperature structural model. Despite the clear difference in the quality of the predictions offered by the room-temperature X-ray data set vs that from 100 K, only the Xe 2 site yields a markedly different O_2 occupancy estimate which reflects the dominant relaxation contribution of a single amide (Ser 108) for which the $\langle 1/r^6 \rangle$ distance to the cavity differs by 0.4 Å between the two crystal structures.

As noted above, little paramagnetically induced relaxation appears to arise from O_2 bound in the distal pocket. However, the larger distance between the distal pocket and nearby amide protons leads to an ~20-fold reduced sensitivity relative to the Xe 4 data. Nevertheless, the O_2 binding constant to the distal pocket appears to be smaller than that of Xe 4. The cavity calculations used in this analysis do not include the distal water of hydration which is present at an occupancy of 0.6. Inclusion of this water eliminates the distal cavity illustrated in Figure 2. As a result, it is expected that whatever relaxation contribution arises from O_2 noncovalently bound to the distal pocket, it comes primarily from the unhydrated form.

On the basis of the congruence between the slower phase of geminate recombination and the exit rate of CO from the Xe 4 site into the protein interior observed by time-resolved Laue diffraction,[22] the distal pocket and Xe 4 site are assigned to the B state while the other three xenon sites are assigned to the C state in the kinetic schemes of Figure 1. Despite the differences observed for the relative O_2 occupancies of the individual cavities predicted by the room temperature vs 100 K X-ray coordinate sets, both sets predict a k_{bc}/k_{cb} value very close to 5. This experimentally determined ratio differs considerably from the value predicted by either the unconstrained sequential ($k_{bc}/k_{cb} = 7.9$) or side path ($k_{bc}/k_{cb} = 1.2$) models (Table 1, entries 1 and 2).

Estimation of CO Migration Kinetics. Although both the side path and sequential models can adequately fit the time course of room-temperature O_2 recombination with the heme, the predicted O_2 migration through the C state differs markedly for the two models. Insight into this process is provided by the time-resolved Laue diffraction of photolyzed CO−myoglobin at room temperature.[22] As noted above, the rate of transfer of CO from the distal pocket Xe 4 region to the Xe 1 ($\tau_{1/2} \sim 70$ ns) is comparable to that deduced for the transfer of O_2 from the B to C state. In addition, the fraction of photodissociated CO in the Xe 1 site reaches ~60% in the time window of 100−400 ns. A similar level of CO transfer to the Xe 1 site was reported in an earlier cryocrystallographic kinetic trapping experiment.[21] As discussed in more detail below, in the time-resolved Laue diffraction study[22] the C state population subsequently decreases at a rate consistent with a ~1.5 μs time constant for CO escape into solvent.

Table 1. Predicted Time Course of CO Migration through B and C States following Photolysis

		C_{max}		
(k_{ba}, k_{bc}, k_{cb}, k_{bs}, k_{cs}) (μs^{-1})	$B_{50\%}$[a] (ns)	%	ns	(1/e)C_{max}[b] (μs)
(5.7, 10.3, 1.30, -, 2.0)[c]	70	61	190	0.84
(5.7, 4.0, 3.30, 6.3, -)[c]	70	24	180	0.84
(6.7, 15.5, 3.10, -, 3.1)[d]	50	58	120	0.56
(5.1, 3.2, 0.64, 4.3, -)[d]	90	40	340	3.3
(6.7, 15.7, 3.14, -, 3.1)[d,e]	50	58	120	0.56
(5.5, 5.7, 1.14, 3.0, -)[d,e]	80	52	350	3.6

[a] Time at which *B* state population decreases to 50% of maximum. An Fe^{2+} recombination rate $k_{ba}/20$ was used for the CO migration simulations. [b] Time at which *C* state population decreases to 37% of maximum. [c] Optimal fit to O_2 geminate recombination data.[7] [d] $k_{bc} = 5k_{cb}$, mean value of parameter sets fitting O_2 geminate recombination data to within 1% rmsd. [e] Distal hydration level of 0.6.

CO reacts with the heme ~20-fold more slowly than does O_2.[44] Given the similar size and low polarity, CO migration can be modeled from the O_2 recombination data by a corresponding reduction in the rate of covalent bond formation k_{ba}. Using the kinetic parameters derived from an optimal fit of the O_2 recombination data to the sequential and side path models, numerical simulations provide estimates for the half-time of CO exit from the B state, the percentage and time of maximal CO buildup in the C state, and the apparent time constant for CO exit from the C state for comparison to the time-resolved Laue diffraction results (Table 1).

The CO migration kinetics predicted from the previously reported[7] optimal fits for the unconstrained sequential (Figure 1a) and side path (Figure 1b) models are given in entries 1 and 2 of Table 1, respectively. The corresponding CO migration behavior predicted when k_{bc}/k_{cb} is constrained to 5.0 is listed in entries 3 and 4. To facilitate comparison in the subsequent discussion, the constrained (k_{ba}, k_{bc}, k_{bs}, k_{cs}) values given are the mean values from a grid search over all parameter sets which fit the reference geminate recombination data to within an experimental uncertainty of 1% rmsd. The sequential model, either unconstrained or with k_{bc}/k_{cb} set to 5.0, yields predictions near the observed maximal C state concentration of 60% (Table 1, entries 1 and 3). In contrast, the side path model predicts a significantly lower value of 24% for the maximal C state concentration (Table 1, entry 2). Incorporation of the constraint of $k_{bc}/k_{cb} = 5.0$ into the side path model increases the predicted maximal C state concentration to 40%. (entry 4).

(44) Henry, E. R.; Sommer, J. H.; Hofrichter, J.; Eaton, W. A. *J. Mol. Biol.* **1983**, *166*, 443−451.

The marked difference in maximal C state concentration predicted by the unconstrained side path vs sequential models has led to the proposal that kinetic crystallography could serve to distinguish between these models.[17] However, introduction of the experimental relative O_2 binding constant of the B state vs C state markedly increases the maximal C state concentration predicted by the side path model. As discussed below, the additional introduction of distal pocket hydration effects yield virtually indistinguishable estimates for the maximal C state concentration from either the sequential or side path models.

Once the constraint of $k_{bc}/k_{cb} = 5.0$ is considered, a far more clear distinction between the sequential and side path models can be drawn. Although the unconstrained versions of both the sequential and side path models predict a similar residence time for CO in the Xe 1 site (Table 1, entries 1 and 2), incorporation of the experimental k_{bc}/k_{cb} constraint results in prediction of a nearly 6-fold difference in the CO residence time (Table 1, entries 3 and 4). It is perhaps initially surprising that the sequential pathway is characterized by short, rather than long, CO residence times in the Xe 1 site. However, the return from the C state to the B state (k_{cb}) is consistently predicted to be as slow or slower than the exit from the protein (either k_{bs} or k_{cs}). Since the C to B state transition is required for emptying the Xe 1 site via the side path model, the corresponding residence time is necessarily longer. This difference in Xe 1 residence time provides a potential experimental means of determining the fraction of CO (and O_2) utilizing each of these two alternate migration pathways. In a similar fashion, the absolute O_2 binding constant for the Xe 1 site predicted from the observed 16 μM^{-1} s^{-1} bimolecular association rate constant[7] is model dependent. A binding constant of 20 M^{-1} is predicted by the sequential model, while this value increases to 30 M^{-1} for the side path model.

In the time-resolved Laue diffraction study,[22] the decay from the maximal CO concentration in the Xe 1 site drops to a plateau level which extends to ~100 μs. The observed CO level in this plateau region is consistent with the 0.15 occupancy factor which is predicted from the estimated binding constant for the Xe 1 site and those authors' estimate of 45 mM total heme in the crystal and 15 mM CO not bound to iron during this time interval. Under steady-state conditions, nearly half of the CO that is not covalently bound should reside in the Xe 1 site, until essentially all of it ultimately rebinds to the heme. The resultant lower CO concentration in solution would lead to a reduced apparent biomolecular association rate constant for rebinding to Fe^{2+} in the crystal as was observed.[22] Furthermore, the nearly equal quantities of CO free in solution and bound in the Xe 1 site implies that, under these conditions, the rate of CO entry into Xe 1 and the rate of CO exit from Xe 1 into the solvent phase are approximately equal. In turn, this predicts that the observed time constant for decay from the maximal CO concentration in the Xe 1 site down to the plateau level will be $\sim^1/_2$ the time constant for the unidirectional transitions. Although the data of Moffatt and co-workers[22] does not precisely define the time course of this decay, the predicted rate of CO exit from the Xe 1 site is approximately 1.5 μs.

As noted above, the biexponential O_2 geminate recombination data yields four experimental parameters while the bimolecular association rate yields a fifth. In contrast, the combined sequential + side path model (Figure 5) needed to characterize

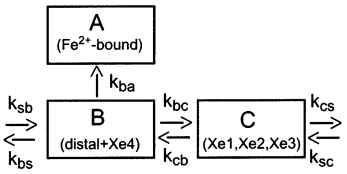

Figure 5. Combined sequential + side path model for myoglobin binding and release of O_2.

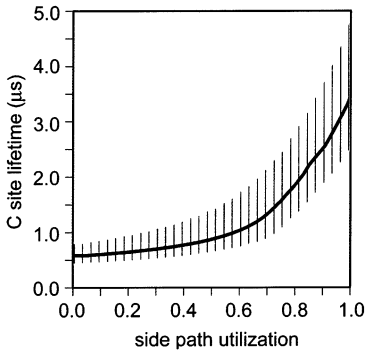

Figure 6. Predicted mean and maximal range of CO lifetimes in the C state as a function of the fraction of the Fe^{2+}-bound population which enters via the histidine gate. The kinetic parameter sets (k_{ba}, k_{bc}, k_{bs}, k_{cs}) of the combined sequential + side path model of Figure 5 were exhaustively searched to determine all combinations consistent with the observed O_2 geminate recombination kinetics to within 1 rmsd of 1%. A relative reactivity of CO vs O_2 of 1/20[44] was assumed. The k_{bc}/k_{cb} value of 5 was used on the basis of the equilibrium O_2 binding data described herein.

the relative fraction of the two migration pathways has six independent variables. The relative O_2 binding measurements reported herein yield an additional experimental constraint, thus rendering analysis of the combined pathway model potentially feasible. However, there is a significant degree of correlation among the variables of the model in terms of the predicted observables. When combined with the experimental uncertainty in the geminate recombination and bimolecular association measurements, a substantial range of values for the individual model parameters are compatible with the observed data. Therefore, rather than relying on only optimized parameter fits to generate an estimate of the fraction of O_2 entering via the sequential vs side path migration, the entire population of parameter sets consistent with the given experimental data was considered. A grid search over all consistent (k_{ba}, k_{bc}, k_{bs}, k_{cs}) sets demonstrates a strong correlation between the fraction of Fe^{2+}-bound O_2 entering via the histidine gate and the estimated time for the C state population decrease to 1/e of the maximal value (Figure 6). This correlation between pathway utilization and the C state lifetime is primarily a function of the equilibrium binding ratio k_{bc}/k_{cb} (set to 5.0) and is only weakly dependent on the assumed reactivity of CO relative to O_2. The 1.5 μs time constant for CO exit from the Xe 1 site estimated from the time-resolved Laue diffraction data[22] applied to the combined sequential and side path model of Figure 5 predicts that a majority of the CO or (O_2) exits via the histidine gate pathway.

Effect of Hydration. The combined sequential + side path model of Figure 5 disregards the potential kinetic effects of the competition between O_2 and water binding in the distal pocket. However, given the experimentally observed occupancy of 0.6 for the distal water of hydration, the effects of this competitive binding can be plausibly incorporated without introducing any additional unconstrained model parameters. In the proposed model, the histidine gate opening is assumed to enable O_2

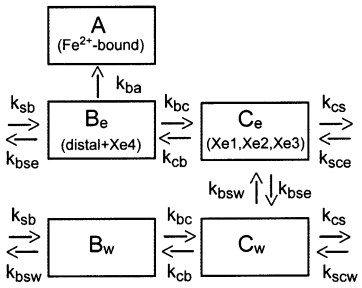

Figure 7. Combined sequential + side path model for myoglobin binding and release of O_2 in which the distal pocket is either otherwise empty (e) or contains a bound water of hydration (w). Covalent binding to iron is assumed to occur only in the absence of distal pocket hydration. The opening of the histidine gate (from the B state to solvent) is assumed to allow for O_2 entry and exit as well as equilibration of the distal hydration state. The relative rate of exit from the B state (k_{bse} vs k_{bsw}) and entry into the C state (k_{sce} vs k_{scw}) is determined by the equlibrium occupancy factor for the water in the distal pocket.

exchange and simultaneous equilibration of water binding in the distal pocket, with the water−distal histidine interaction controlling the relative rate of gate opening. The rate of O_2 entry via the histidine gate is assumed to be independent of the resultant state of distal hydration. Experimental support comes from the 5.7 μs^{-1} rate of H_2O binding to the Fe^{3+} in metmyoglobin after the sixth coordination site is vacated by photolysis of the NO complex.[45] This study found that the activation energy barrier of 42 ± 3 kJ/mol for water entry equals that observed for the escape of photolyzed CO. Analogous studies for the Fe^{2+} form are less straightforward since in this case the lack of covalent bonding between water and the iron atom results in a much weaker spectral signature. Nevertheless, time-resolved optical absorption spectroscopy indicates a 3 μs^{-1} rate process ascribed to rehydration dynamics.[46] The CO buildup in the Xe 1 site reported by cryocrystallography occurs simultaneously with an increase in electron density in the distal pocket which the authors interpret as rehydration.[21] The pH dependence of the "open" and "closed" subpopulations of CO−myoglobin correlates with protonation of the distal histidine[47] and indicates an interconversion rate of 1.4 μs^{-1} at 0 °C.[48] At pH 7, there is ∼2% open form,[48] implying a histidine open-state lifetime of ∼10 ns, which molecular simulations[15] predict to be sufficient for complete O_2 exit from the distal pocket. Consistent with the binding affinity of the distal pocket for O_2 appearing to be significantly less than that of the Xe 4 site, both k_{bc} and k_{cb} are assumed to be independent of the state of distal pocket hydration.

In the proposed hydrated model (Figure 7) distal hydration is assumed to block covalent binding of O_2 to the iron so that only the unhydrated B_e state can transfer O_2 to the A state. Incorporating the O_2 equilibrium binding constraint k_{bc}/k_{cb} and the water occupancy of 0.6 (Table 1, entry 6) improves the estimate of the maximal CO concentration in the C state as compared to the unhydrated side path model. On the other hand, introduction of hydration has little effect on the predicted rate of CO exit from the Xe 1 site for either the sequential or side path model. This underscores the fact that the O_2 equilibrium binding constraint k_{bc}/k_{cb} predominantly determines the dependence of the C state lifetime on the pathway of egress. However as seen in Figure 8, the correlation of residence time of CO in the C state vs the fractional utilization of the histidine gate is markedly more linear for the hydrated model as compared to the graph of the unhydrated model in Figure 6. In the absence of competitive water binding, the contribution from the sequential migration tends to dominate the predicted C state lifetime since all of the CO following that path must pass through the C state. In contrast, for the unhydrated side path model only 48% of the photolyzed CO is predicted to enter the C state. As a result, the C state lifetime is comparatively insensitive to the fraction of histidine gate entry until that fraction becomes fairly large. When distal hydration is incorporated into the side path model, 65% of the photolyzed CO is predicted to migrate into the C state. Thus, at smaller fractions of histidine gate entry, side path migration makes a substantial contribution to the predicted overall C state lifetime.

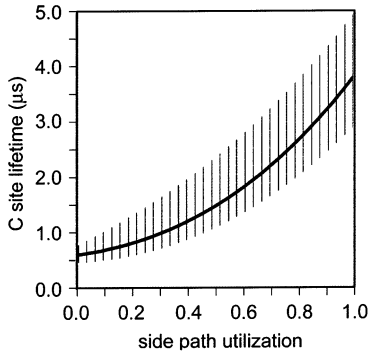

Figure 8. Predicted mean and maximal range of CO lifetimes in the C state as a function of the fraction of the Fe^{2+}-bound population which enters via the histidine gate in competition with water binding in the distal pocket. The kinetic parameter sets (k_{ba}, k_{bc}, k_{bs}, k_{cs}) of the combined hydrated sequential + side path model of Figure 7 were exhaustively searched to determine all combinations consistent with the observed O_2 geminate recombination kinetics to within 1 rmsd of 1%.[7] The distal hydration occupancy of 0.6[23,24] and a relative reactivity of CO vs O_2 of 1/20[44] were assumed. The k_{bc}/k_{cb} value of 5 was used on the basis of the equilibrium O_2 binding data described herein.

Discussion

A role for the distal heme cavity in accommodating the O_2 molecule covalently bound to iron appears straightforward. In contrast, a potential selective advantage in O_2 transport arising from the evolutionarily conserved[49] secondary cavities of myoglobin, most particularly Xe 1, has remained unclear. Indeed, alternate physiological roles for these cavities in NO metabolism have been proposed.[50] A physiological role for the secondary cavities in the binding competition between water and O_2 for the distal pocket can be proposed by reference to the side path migration model. In the absence of a C state, when both water and oxygen enter from the solvent phase together, reopening of the histidine gate and O_2 exit would precede the next potential iron binding event. Migration of O_2 into the C state allows for reequilibration of distal hydration before the O_2 molecule reenters the B state. The optimal kinetic parameters of the hydrated side path model predict that, in the absence of

(45) Cao, W.; Christian, J. F.; Champion, P. M.; Rosca, F.; Sage, J. T. *Biochemistry* **2001**, *40*, 5728−5737.
(46) Esquerra, R. M.; Goldbeck, R. A.; Kim-Shapiro, D. B.; Kliger, D. S. *Biochemistry* **1998**, *37*, 17527−17536.
(47) Morikis, D.; Champion, P. M.; Springer, B. A.; Sligar, S. G. *Biochemistry* **1989**, *28*, 4791−4800.
(48) Tian, W. D.; Sage, J. T.; Champion, P. M.; Chien, E.; Sligar, S. G. *Biochemistry* **1996**, *35*, 3487−3502.
(49) Suzuki, T.; Imai, K. *Cell. Mol. Life Sci.* **1998**, *54*, 979−1004.
(50) Frauenfelder, H.; McMahon, B. H.; Austin, R. H.; Chu, K.; Groves, J. T. *Proc. Natl. Acad. Sci. U.S.A.* **2001**, *98*, 2370−2374.

a C state, only 25% of the O_2 which enters the B state from the solvent becomes bound to iron before it has a chance to exit back into the solvent phase. When the C state is incorporated into the migration pathway, the overall efficiency of O_2 binding to the iron increases 1.5-fold to 37%.

The utility of this mechanism imposes severe constraints on the rate constants. If a substantial fraction of O_2 is to be affected, the rate of B to C transfer must compete favorably with exit to solvent. However, if the return to the B state is fast compared to k_{bs}, reequilibration of hydration cannot be achieved, and the B and C states effectively merge to a common kinetic state. The ability to integrate the kinetic effects of competition from the distal hydration in a manner consistent with the observed O_2 geminate recombination data suggests that the multiexponential character of the rebinding process reflects not only the return of O_2 from the secondary cavities to the distal pocket but also the time dependence of water penetration into the distal cavity.

It may be noted that increasing the volume of the Xe 1 cavity by alanine substitutions at either residue 104 or 138 also results in an increase in the O_2 bimolecular association rate constant. In contrast, filling that cavity by a tryptophan substitution at either position or by applying 12 atm Xe pressure leads to a ~40% reduction in the association rate.[7] Such behavior is not anticipated from a simple unhydrated side path model, although it is obviously compatible with a sequential pathway. On the other hand, these changes in association rate occur with modest effect on the geminate recombination fraction consistent with the hydrated side path model but unexpected from a sequential pathway.

Hemoglobin-catalyzed oxidation of the cellular regulator NO has led to systemic vasoconstriction in clinical use of blood substitutes based on extracellular hemoglobin.[51] Certain mutations that reduce the volume of the distal pocket for both the α and β chains of hemoglobin have been found to reduce its reactivity with NO and in turn decrease the vasoconstriction arising from the extracellular hemoglobin.[52] The combination of equilibrium O_2 binding measurements and CO and/or O_2 migration data provides a means of determining the relative kinetic contributions of the histidine gate vs secondary cavity pathways to the entry and egress of such gases. Such information will significantly inform the rational design of globin-based blood substitutes for which O_2 k_{on} and k_{off} rates as well as the overall equilibrium constant are of critical importance.

Acknowledgment. We thank Robert G. Bryant for useful discussions. We acknowledge the use of the Wadsworth Center NMR Facility. This work was supported in part by NIH Grant GM 38779 (D.M.L.).

JA028064S

(51) Patel, R. P. *Free Radical Biol. Med.* **2000**, *28*, 1518−1525.
(52) Doherty, D. H.; Doyle, M. P.; Curry, S. R.; Vali, R. J.; Fattor, T. J.; Olson, J. S.; Lemon, D. D. *Nat. Biotechnol.* **1998**, *16*, 672−676.